How to cite: *Angew. Chem. Int. Ed.* **2023**, *62*, e202308790
doi.org/10.1002/anie.202308790

Semihydrogenation Catalysis

Catalytic Alkyne Semihydrogenation with Polyhydride Ni/Ga Clusters

*Maximilian Muhr, Hao Liang, Lars Allmendinger, Raphael Bühler, Fabrizio E. Napoli, Dardan Ukaj, Mirza Cokoja, Christian Jandl, Samia Kahlal, Jean-Yves Saillard, Christian Gemel, and Roland A. Fischer**

Abstract: The bimetallic, decanuclear Ni_3Ga_7-cluster of the formula $[Ni_3(GaTMP)_3(\mu^2\text{-}GaTMP)_3(\mu^3\text{-}GaTMP)]$ (**1**, TMP = 2,2,6,6-tetramethylpiperidinyl) reacts reversibly with dihydrogen under the formation of a series of (poly-)hydride clusters **2**. Low-temperature 2D NMR experiments at −80 °C show that **2** consist of a mixture of a di- ($\mathbf{2_{Di}}$), tetra- ($\mathbf{2_{Tetra}}$) and hexahydride species ($\mathbf{2_{Hexa}}$). The structures of $\mathbf{2_{Di}}$ and $\mathbf{2_{Tetra}}$ are assessed by a combination of 2D NMR spectroscopy and DFT calculations. The cooperation of both metals is essential for the high hydrogen uptake of the cluster. Polyhydrides **2** are catalytically active in the semihydrogenation of 4-octyne to 4-octene with good selectivity. The example is the first of its kind and conceptually relates properties of molecular, atom-precise transition metal/main group metal clusters to the respective solid-state phase in catalysis.

Introduction

Molecular compounds with direct bonds between transition metals (TM) and group 11–13 metals (E) exhibit characteristically modified reactivity with respect to their monometallic components.[1] Especially complexes of late TMs coordinated by E(I) (E=Al, Ga, In) ligands have been investigated in the context of bond activation reactions. The complex $[Cp^*Rh(CH_3)_2(GaCp^*)]$, for example, shows a facile intermolecular C–C bond activation of a Cp* ligand ($Cp^* = C_5Me_5$).[2] Intramolecular C–H bond activations are observed for $[M(AlCp^*)_5]$ (M=Fe, Al).[3] The intermolecular C–H and Si–H activation of C_6H_6 and $HSiEt_3$ are mediated by unsaturated intermediates such as $[Ni(AlCp^*)_3]$[4] and $[Ru(GaCp^*)_3(H)_2]$.[5] These reactivities can often be attributed to cooperative effects of the two metals and are a consequence of the high donor capacity of the ECp* ligand, resulting in strongly polarized $TM^{\delta-}\text{-}E^{\delta+}$ bonds. No catalytic reactions, however, have been identified so far.[6] Herein we report a first example that puts the above introduced properties of TM complexes or clusters stabilized by E(I) ligands with direct TM–E bonds into value for catalytic reactions: The Ni/Ga cluster $[Ni_3(GaTMP)_7]$ (**1**, TMP = 2,2,6,6-tetramethylpiperidinyl) reversibly reacts with hydrogen, enabling the catalytic semihydrogenation of alkynes to alkenes (Figure 1). The use of the cluster protecting amide ligand is of crucial importance here. Related Ni/Ga clusters protected by Cp* are known, however, these undergo Cp*-transfer reactions from Ga to Ni, leading to deactivation of the Ni centres.[7] In contrast, the η^1-amide preferably coordinates to Ga and the Ga-amide bond is stable even under hydrogenolytic conditions.[8] We identified a series of

[*] Dr. M. Muhr, R. Bühler, F. E. Napoli, Dr. D. Ukaj, Dr. M. Cokoja, Dr. C. Jandl, Dr. C. Gemel, Prof. Dr. R. A. Fischer
Technical University of Munich, TUM School of Natural Sciences, Department of Chemistry, Chair of Inorganic and Metal-Organic Chemistry, Lichtenbergstraße 4, 85748 Garching (Germany)
and
Catalysis Research Centre, Technical University Munich, Ernst-Otto-Fischer Straße 1, 85748 Garching (Germany)
E-mail: roland.fischer@tum.de
H. Liang, Dr. S. Kahlal, Prof. Dr. J.-Y. Saillard
Univ Rennes, CNRS, ISCR-UMR 6226, 35000 Rennes (France)
Dr. L. Allmendinger
Department of Pharmacy, Ludwig-Maximilians-University Munich, Butenandtstrasse 7, 81377 Munich (Germany)

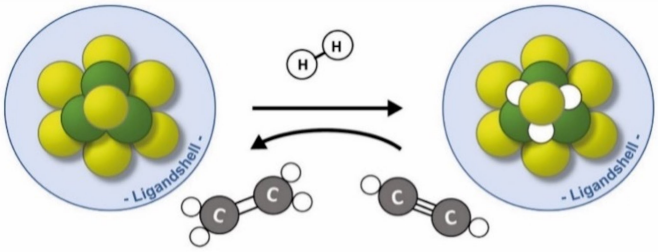

Figure 1. Conceptual Scheme depicting the reaction of the alkylamide ligand protected cluster $[Ni_3(GaTMP)_7]$ (**1**, left) with H_2 to yield the (poly−)hydride clusters $[Ni_3(GaTMP)_7(H)_x]$ (**2**, right; $x = 2,4,6$). Color code: *yellow*, Ga; *green* Ni; *white*, H; *blue*, TMP ligand shell (TMP = 2,2,6,6-tetramethylpiperidinyl). The (poly−)hydride clusters **2** (right) enable catalytic semihydrogenation of alkynes to alkenes. The structures of **1** and **2** may serve as a molecular model for the catalytically active sites at the surface of the Ni_5Ga_3 solid-state phase.

(poly-)hydride clusters $[Ni_3(GaTMP)_7(H)_x]$ (**2**, $x=2,4,6$) as the key species for driving the catalytic alkyne semihydrogenation and succeeded in accurately determining their structures by 2D NMR methods in conjunction with DFT calculations. The structural assignment allows for identification of the non-innocent role of the Ga ligands.

We like to put our work into the context of conceptually linking the molecular cluster and the solid-state chemistry of intermetallics.[1] Intermetallic solid-state materials represent an important class of industrially relevant catalysts. A Pd/Ag alloy is typically used in the purification of ethylene feedstocks from trace acetylene impurities.[9] Generally, the dilution of the catalytically more active TM in a matrix of catalytically much less active E leads to improved selectivity due to the formation of isolated TM atoms or small TM clusters at the catalysts surface.[10] Intermetallic NiGa phases have been investigated as catalysts for the alkyne semihydrogenation, especially the Ni_5Ga_3 phase exhibits excellent balance of activity and selectivity.[11] This motivated us to explore the chemistry of ligated, atom-precise clusters with well-defined active centres. From a heuristic point of view, catalytic reactivity patterns and intermediates can be studied on a molecular level and can potentially be linked to structurally related solid-state materials.

Results and Discussion

The stoichiometric reaction of $Ni(cod)_2$ with $[GaTMP]_4$[12] at 60 °C in toluene gives the new, dark purple Ni_3-cluster $[Ni_3(GaTMP)_7]$ (**1**, Figure 2). The already reported, related

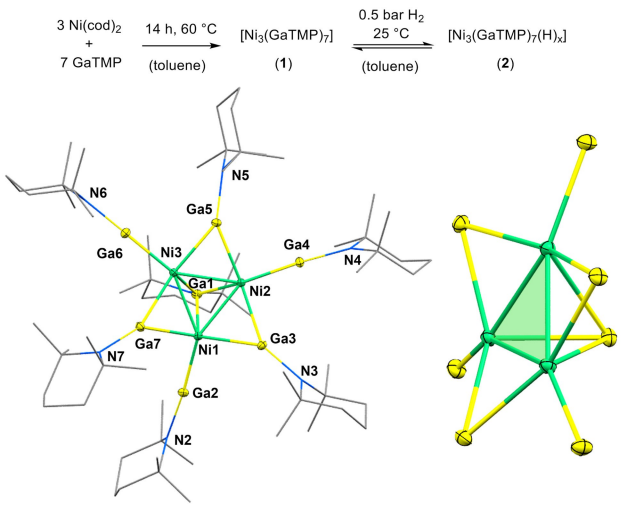

Figure 2. *Above*: Reaction scheme of the cluster synthesis of **1** and the conversion by H_2 addition to yield the (poly-)hydridic species **2**.— *Below*: The molecular structure of **1** in the solid-state is shown left (thermal ellipsoids are given at the 50% probability level).[25] TMP ligands are given in wireframe depiction and H atoms are omitted for clarity. Selected bond length (Å) and angle (deg) ranges: Ni–Ni 2.383–2.396, Ni–μ^1-Ga 2.175–2.184, Ni–μ^2-Ga 2.214–2.227, Ni–μ^3-Ga. 2.314–2.411; Ni–Ni–Ni 59.7°–60.3°. The Ni/Ga metal core structure of **1** is shown at the right side. TMP ligands are omitted. Green plane highlights the well-accessible Ni_3 triangle.

Ni_2-cluster $[Ni_2(GaTMP)_7]$ is observed by LIFDI-MS (Figures S35–S36) as an intermediate in this reaction.[13] Accordingly, the reaction of pure $[Ni_2(GaTMP)_7]$ with $Ni(cod)_2$ leads to **1**. Cooling reaction solutions of **1** to −30 °C overnight, yields dark purple single crystals of space group $P2_1/n$. Single crystal X-ray diffraction (SC-XRD) reveals the molecular structure of **1** in the solid state: A central Ni_3-triangle is coordinated by three terminal GaTMP, three Ni_2-edge bridging μ^2-GaTMP as well as one capping μ^3-GaTMP ligand over one side of the Ni_3-triangle (Figure 2). The overall structure of **1**, written as $[Ni_3(GaTMP)_3(\mu^2\text{-}GaTMP)_3(\mu^3\text{-}GaTMP)]$ is very similar to that of $[Ni_3(i\text{Pr}_2\text{Im})_3(\mu^2\text{-}CO)_3(\mu^3\text{-}CO)]$ ($i\text{Pr}_2\text{Im}$ = 1,3-di(isopropyl)-imidazol-2-ylidene).[14] This similarity further underlines the comparable coordination properties of the formally two electron donating GaTMP with CO and N-heterocyclic carbene (NHC) ligands.[13a] The Ni_3 triangle is almost perfectly unilateral (Ni–Ni distances: 2.383–2.396 Å, Ni_3 angles; 59.7°–60.3°) and in good agreement with other Ni clusters known in literature.[7b,14–15] The terminal and bridging μ^2-GaTMP ligands are almost in plane with the Ni_3-triangle. The terminal Ni–Ga (2.175–2.184 Å) bonds are distinctly shorter than the Ni–μ^2-Ga (2.214–2.227 Å) and the Ni–μ^3-Ga (2.314–2.411 Å) bonds, which is in line with other Ga^I stabilized transition metal cluster compounds.[7b,13a,16] The ^{1}H NMR (Figures S1–S2) and ^{13}C NMR spectra (Figures S3–S4) of **1** in toluene-d_8 are consistent with the molecular symmetry in the solid state structure: ^{1}H signals can be divided into two groups with a ratio of 3:4, indicating a fluxional process exchanging the μ^2- and μ^3-bridging GaTMP ligands. All ^{1}H and ^{13}C chemical shifts are in similar ranges with respect to $[Ni_2(GaTMP)_7]$.[13a] A detailed assignment of the NMR data of **1** can be found in the Supporting Information.

The coordination environment of the Ni centers in **1** suggests some reactivity towards small molecules. While one face of the Ni_3 triangle is shielded by bulky GaTMP ligands, the other remains open and accessible towards potential substrates. At the same time, the electron donating Ga^I ligands generate electron-rich nickel centers and introduce $Ni^{\delta-}$–$Ga^{\delta+}$ bond polarization that should facilitate oxidative addition reactions. Indeed, when a solution of **1** in toluene-d_8 is subjected to 1 bar H_2, a series of new hydride clusters **2** is formed in equilibrium with **1**, namely $[Ni_3(GaTMP)_7(H)_x]$ ($\mathbf{2_{Di}}$, $x=2$; $\mathbf{2_{Tetra}}$, $x=4$; $\mathbf{2_{Hexa}}$, $x=6$). In the ^{1}H NMR spectrum of **2** at room temperature, only one broad, coalesced singlet at −8.66 ppm is present (Figures S7–S10). Likewise, the aliphatic region gives rise to one new set of TMP signals, indicating fluxional processes which exchange hydride ligands (intermolecularly) as well as TMP ligands (inter- or intramolecularly).

As indicated by the integral ratios of the TMP ligands, the equilibrium can be shifted from **1** to **2** with increasing H_2 pressure (ratio **1/2**: 3.4/1 at 1 bar, 0.6/1 at 3 bar; NMR at r. t. after 15 min reaction; see Figure S26). The hydride formation is fully reversible: When H_2 is removed from solutions containing **2**, e.g. by purging with inert gas, only signals as those of **1** can be detected (Figure S30–31). The reversible nature of the H_2 activation and hydride coordination, as well

as the fact that more than one equivalent of hydrogen is activated, is further supported by a H/D-exchange experiment: Pressuring a sample of **1** in toluene-d_8 consecutively with D_2 (1.5 bar) and H_2 (3 bar), results in the observation of a significant amount of HD (4.51 ppm)[17] in the ^{1}H NMR spectrum (Figure S25). Single crystals of **2** suitable for (low-temperature) X-ray diffraction studies could not be obtained and likewise the lability of **2** prohibited characterization by LIFDI-MS. The structural assignment of **2** was thus based on detailed NMR spectroscopic studies. At −80 °C the coalescent hydride signal of **2** [$Ni_3(GaTMP)_7(H)_x$] splits into five distinct singlets at −6.09, −7.58, −8.15, −9.02 and −9.31 ppm (Figures S11–S14). According to their T_1 relaxation time (500–700 ms), all signals are related to classic metal-hydride bonding (Figure S22).[18] A ^{1}H,^{1}H COSY spectrum at −80 °C reveals coupling between the hydrides represented by the signals at −7.58 and −9.31 ppm (integral ratio 1:1) as well as coupling between the hydrides represented by the signals at −5.97, −8.32 and −9.02 ppm (integral ratio 1:1:2). This points to a dihydride complex $\mathbf{2_{Di}}$ and as well as to a tetrahydride complex $\mathbf{2_{Tetra}}$, respectively (Figure S15–16). The four remaining small peaks at −6.98, −7.13, −7.78 and −9.44 ppm are attributed to the hexahydride complex $\mathbf{2_{Hexa}}$ under the assumption that further related signal(s) may be covered by the broad peaks of $\mathbf{2_{Di}}$ and $\mathbf{2_{Tetra}}$. Notably no correlated COSY cross peaks are found for $\mathbf{2_{Hexa}}$, probably due to its low concentration and resulting small signal intensities. Surprisingly, the H_2 pressure does not influence the quantitative distribution of signals of **2**, at least in the experimentally accessible range of 1–3 bar.

In order to gain insight into the location of the hydride ligands in the three (poly)hydride complexes of **2**, a computational search for their low-energy isomers was performed at the DFT level of theory (computational details given in Supporting Information). Several local minima could be identified for $\mathbf{2_{Di}}$ as well as for $\mathbf{2_{Tetra}}$. The isomers differ in the exact distribution of the hydride ligands over the Ni_3Ga_7 framework. Hydride ligands were found in terminal Ni–H, μ^2-bridging (Ni–H–Ni, Ni–H–Ga) positions as well as μ^3-(H–Ni_3)-bridging positions. A Figure depicting all computationally identified isomers of **2** as well as their calculated relative energies are given in the Supporting Information (Figure S53, S54, S57–S59; Table S5). The Ni–Ni distances in **2** are distinctly longer than those in **1**, whereas the Ni–Ga bond lengths remain almost the same. Notably, the μ^2-hydride bridged Ni–Ni bond in $\mathbf{2_{Di}}$ is about 0.2 Å shorter as the average of all other Ni–Ni bonds. For $\mathbf{2_{Di}}$, four energetic minima were located, two of which exhibit a hydride distribution reflecting the unsymmetric nature of the ^{1}H NMR spectrum (two signals, integral ratio 1:1). In both structures one Ni–Ni edge is μ^2-bridged by a hydride, while the second hydride is terminally coordinated to the remaining Ni atom, either on the same (***cis*-$\mathbf{2_{Di}}$**) or the opposite side (***trans*-$\mathbf{2_{Di}}$**, +3.7 kcal/mol) of the Ni_3 triangle. In the case of $\mathbf{2_{Tetra}}$ only one isomer was found with a suitable symmetry reflecting the 1:1:2 integral ratio observed in the hydridic region of the ^{1}H NMR spectrum. For $\mathbf{2_{Hexa}}$ only one minimum structure has been found, with unsymmetrically hydride distribution, featuring three terminal Ni–H and three μ^2-bridged Ni–H–Ga moieties (Figure S43).

The calculated structures were spectroscopically confirmed by phase-sensitive NOESY experiments at −80 °C (Nuclear Overhauser Effect SpectroscopY; Figure S17). However, a clear discrimination between the NOE signals of the hydrides in spatial proximity and signals due to chemical exchange (EXSY) was not unambiguously possible. Probably this is due to slow molecular tumbling rates at such low temperatures, leading to fast relaxation rates and consequently yielding negative NOEs, which are showing the same sign as those arising from chemical exchange. Thus, phase-sensitive ROESY (Rotating Frame Overhauser Effect SpectroscopY) experiments were performed (Figures S18–S21). Regardless of the relaxation rate, they give antiphase cross peaks with respect to the diagonals for ROEs and respective cross peaks with the same phase as the diagonals for signals originating from chemical exchange. This in consequence enables to distinguish between signals related to either proximity or to chemical exchange. It is worth mentioning that the results from the ROESY spectrum were in good accordance with the initially performed NOESY spectra. The ROESY spectrum allows a clear discrimination of different calculated structures according to the hydride distribution, in particular with respect to the relative intramolecular proximity of hydride ligands. While in ***trans*-$\mathbf{2_{Di}}$** the H–H distance is calculated to be 4.22 Å, this distance is only 3.18 Å in the optimized structure of ***cis*-$\mathbf{2_{Di}}$** (Figure 3), suggesting that the experimentally observed isomer of $\mathbf{2_{Di}}$ is ***cis*-$\mathbf{2_{Di}}$**, which is also the energetically more favorable isomer. The structure of $\mathbf{2_{Tetra}}$ can be assigned in a similar manner: The energetically most favorable isomer, according to DFT, contains three μ^2-Ni–H–Ga, bringing each Ni to the μ^3-Ga, as well as one terminal Ni–H—resulting in an overall C_s symmetric structure (Figure 3). The ROE cross-peaks of $\mathbf{2_{Tetra}}$ are only observed for hydrides with a H–H distance of 3.01 Å and 3.23 Å, respectively, but not between the hydrides with a distance of 4.43 Å. The minimum structure of $\mathbf{2_{Tetra}}$ is in line with the symmetry observed in the ^{1}H NMR spectrum, as well as the ROESY cross peaks. For $\mathbf{2_{Hexa}}$ only one local minimum structure could be found (Figure S43). In this structure, the six hydridic ligands are

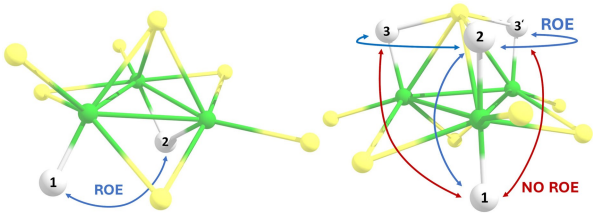

Figure 3. Calculated structures of $\mathbf{2_{Di}}$ and $\mathbf{2_{Tetra}}$ with interpretation for respective ROESY signals. Intramolecular hydride-hydride distance is the reason for ROE signals. Blue arrow—ROE signal; red arrow—no ROE signal. TMP ligands omitted for clarity, Ni (green), Ga (yellow) and H (white). *Left*) Calculated structure of ***cis*-$\mathbf{2_{Di}}$** with d_{12} = 3.18 Å (ROE signal). *Right*) Calculated structure of $\mathbf{2_{Tetra}}$ with d_{12} = 3.01 Å (ROE signal), $d_{23/3'}$ = 3.23 Å (ROE signal) and $d_{13/3'}$ = 4.43 Å (no ROE signal).

unsymmetrically coordinated which agrees with the four distinct small signals in the ^{1}H NMR spectrum, considering that the two remaining signals could be covered by the broad signals of $\mathbf{2}_{\mathbf{Di}}$ and $\mathbf{2}_{\mathbf{Tetra}}$. It should be noted, however, that no hydridic ROE signals were detected for $\mathbf{2}_{\mathbf{Hexa}}$, presumably due to its low concentration, and therefore a clear deduction of the structure is not possible. Interestingly, EXSY cross peaks are found between the signals of $\mathbf{2}_{\mathbf{Tetra}}$ (−8.3 and −9.0 ppm) and two of the signals assigned to $\mathbf{2}_{\mathbf{Hexa}}$ (−6.9 and −7.1 ppm), respectively, indicating intermolecular hydride exchange between the two species (Figure S21). No EXSY signal between free H_2 and $\mathbf{2}_{\mathbf{Tetra}}$ or $\mathbf{2}_{\mathbf{Hexa}}$ are observed. Notably, all hydride signals of **2** show ROE cross peaks to the TMP methyl signals, including the hydride signals attributed to $\mathbf{2}_{\mathbf{Hexa}}$. Most interestingly, the high hydrogen load of $\mathbf{2}_{\mathbf{Tetra}}$ does not prevent the cluster from further hydrogen uptake. We attribute this feature to the involvement of the non-innocent Ga ligands, which serve as 'storage sites' for the hydrides (Figure 3) and thus keeping the Ni_3 site accessible for additional hydrogen.

Our DFT calculations are consistent with a flat potential energy surface for hydride fluxionality. For example, the interconversion of $\boldsymbol{cis}$-$\mathbf{2}_{\mathbf{Di}}$ into two different isomers, including *cis*/*trans* isomerization of the hydrides, is associated with free energy barriers of 6.6 and 8.0 kcal/mol, respectively. (Figure S55–56).

This hydride mobility on the cluster surface is also characteristic for hydrogen atoms at catalytically active TM nanoparticles[19] and heterogeneous surfaces.[20]

The catalytic activity of **1** in the semihydrogenation of 4-octyne (Figure 4) has been examined by in situ ^{1}H NMR spectroscopy. An NMR tube containing a reaction solution of 4-octyne, mesitylene (internal standard) and 3 mol% **1** in toluene-d_8 was pressurized at 0 °C with 0.5 bar of H_2. The solution was constantly kept at 0 °C and ^{1}H NMR spectra were recorded in 30 min intervals. After 8 h, ca. 50 % of the alkyne is converted with high selectivity (90 %) for the alkene (5 % *n*-octane; turnover number [TON] = 16.7; turnover frequency [TOF] = 2.1 h^{-1}). The alkene concentration reaches a maximum of ca. 67 % after 20 h, however, accompanied by increasing alkane formation (ca. 20 % alkane; selectivity 77 %; TON = 26.0; TOF = 1.3 h^{-1}). Note that, related studies at Ni/Ga nano-colloids or nanocrystals yield similar semihydrogenation selectivity (Table S4).[11a–c] Determination of the alkene *cis*/*trans* ratio is not possible by NMR (Figure S39), due to partial overlap of all signals. Nonetheless, a substantial *cis* excess can be concluded from combining NMR and GC-FID (Gas Chromatography Flame Ionization Detection) data (Figure S43). In situ monitoring (^{1}H NMR) of the reaction under catalytic conditions shows the presence of **1**, **2** as well as the substrates only. No other species or intermediates could be identified. When treating **1** with 4-octyne in the absence of hydrogen all signals remain unchanged, with respect to the spectra of the pure compounds. We suggest the coordination of the alkyne to **2** over the open face of the Ni_3 triangle in some fashion, however, we cannot determine which species, are the catalytically active one(s). The presence of 4-octyne does not change the quantitative ratio of the three polyhydride species when cooling the reaction solution down to −80 °C, where no further catalytic activity is observed. We want to emphasize that the outcome of the catalytic reaction is extremely sensitive to air and moisture. Only when the catalysis is performed in highly clean, strictly de-hydrated NMR tubes, reproducible results are obtained. Nevertheless, catalyst degradation is always observed to some extent (ca. 20 % after 24 h catalysis, Figure S42). The major decomposition product is TMPH, as observed by in situ ^{1}H NMR spectroscopy, which is formed parallel to dark precipitate. After full conversion of 4-octyne, **1** and **2** are still present (Figure S40–S41). To exclude significant catalytic contribution of colloidal Ni or NiGa particles, which may form on the course of the catalysis, the experiment was repeated in the presence of an excess of elemental mercury (Figure S44), well-known to amalgamate metal particles (especially Ni containing particles).[21] Unchanged reaction rates indicate that metal particles are not influencing the rate of the catalytic reaction. Due to the so far limited experimental information on key intermediates, a rigorous computational modeling of the catalytic cycle exceeds the scope of this work. Nevertheless, we like to suggest that the structure of $\mathbf{2}_{\mathbf{Tetra}}$ (Figure 3) would allow for bimetallic cooperativity and an essential role of the Ga in the catalytic cycle. The μ^3-Ga would serve as the 'storage site' for the hydrides, vacating the open Ni_3 site for further substrate coordination. This synergetic function of the Ni and Ga sites would not be possible with chemically innocent spectator ligands, such as CO, NHCs or phosphines.

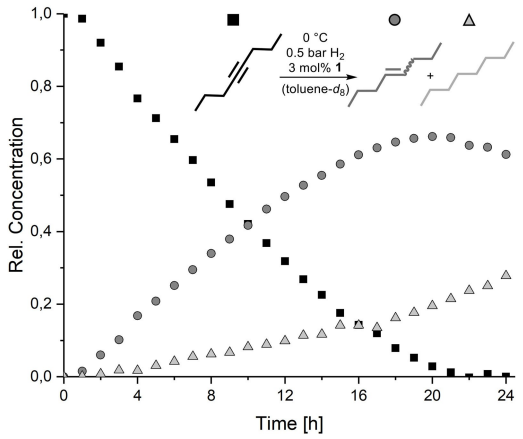

Figure 4. Relative concentrations of the catalytic substrates vs. time. 4-octyne (black, square), 4-octene (dark grey, circle), *n*-octane (light grey, triangle) under given reaction conditions.

In order to gain insight into the thermodynamic parameters of the catalytic process, we studied the coordination of acetylene to $\mathbf{2}_{\mathbf{Tetra}}$ in silico (Figure S60). The formation of a coordination adduct of ethyne and $\mathbf{2}_{\mathbf{Tetra}}$ across one Ni–Ni bond (Figure 5) is indeed an exergonic process (ΔG = −4.4 kcal/mol), whereas coordination of ethene is endergonic (ΔG = 25.4 kcal/mol). This is in good agreement with the experimental result, since this is a key requirement for a semihydrogenation catalyst.[11d] The sum of acetylene coordination, alkyne hydrogenation and hydrogen activation from

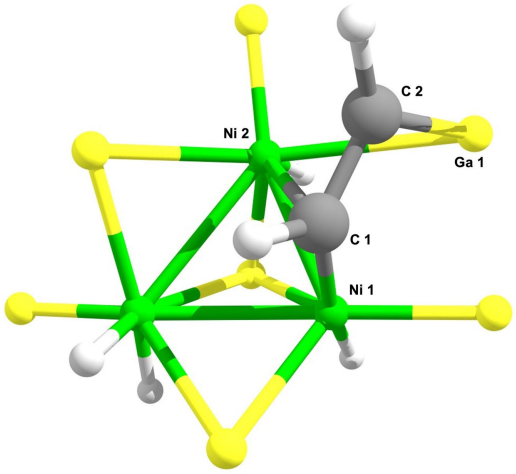

Figure 5. DFT-optimized geometry of the 2_{Tetra}-(C_2H_2) adduct, which shows pronounced Ga–C interactions. Selected bond length (Å): Ga1–C1 1.950, Ni1–C1 1.902, Ni2–C1 2.090, C1–C2 1.407.

2_{Tetra}-(C_2H_2) to **2_{Tetra}-(C_2H_4)** is also exergonic ($\Delta G = -7.2$ kcal/mol; Table S7). Most interestingly the minimum structure of the ethyne adduct **2_{Tetra}-(C_2H_2)** exhibits a distinctly short Ga–C distance (1.950 Å). Such σ-type interactions between ethyne and the electropositive metal (e.g., Ga) are known from solid-state intermetallics catalysis (e.g. Pd_2Ga), as identified by DFT calculations.[20,22]

Extending the substrate scope to 3-hexyne (internal alkyne) resulted in slightly faster catalysis and a slight loss of selectivity (at maximum alkene concentration). The alkene concentration reaches a maximum of ca. 50 % after 11 h, along with ca. 15 % alkane (selectivity 71 %; TON = 21.6; TOF = 2.0 h^{-1}; Figure S46). We attribute this small change to steric influences. This is in line with the incomplete conversion of the relatively hindered/bulky substrate 1,2-diphenylacetylene (ca. 20 % conversion after 24 h; Figure S47). In presence of the terminal alkyne 1-octyne the cluster **1** decomposes under formation of dark solutions as well as a dark precipitate within a few minutes. The LIFDI mass spectrum of the solution reveals oligomerization of the substrate (Figure S49). The decomposition of **1** is presumably a consequence of the C–H acidity of terminal alkynes. Taking into account that acetylides are good cluster stabilizing ligands,[23] we assume cluster growth under these conditions, which is also in line with patterns at higher masses in the mass spectrum. Using the much bulkier triisopropylsilyl-acetylene (TIPSA) as substrate in stoichiometric amounts allows to observe a peak at $m/z = 1826.4338$ in the LIFDI mass spectrum (Figure S50–S51), attributable to the calculated pattern of a TIPSA-acetylide adduct of **1** (calc. $m/z = 1826.4292$). Adding an excess (33 eq) of TIPSA to **1** leads to decomposition, as observed in the in situ LIFDI mass spectrum (Figure S52).

Conclusion

Our data confirm the relationship of our Ni/Ga clusters **1** and **2** to well-known intermetallic Ni/Ga solid-state catalysts for alkyne semihydrogenation. This study is a proof-of-concept that bimetallic clusters can be regarded as molecular mimics of intermetallic solid-sate surfaces. This allows for applying the full spectrum of analytical methods well established for the investigation of molecular processes in solution (1D and 2D NMR, mass spectrometry, SC-XRD, etc.). Specifically the triangular Ni_3 structural motif in **1** is reminiscent of the Ni_5Ga_3 phase, which shows improved catalytic properties with respect to bulk Ni or the Ni_1Ga_1 phase.[11a] The accurate localization of the hydride ligands in **2** by 2D NMR methods and DFT serves as an example. We anticipate our work to stimulate further studies on the structure/reactivity relationships of bimetallic clusters at the atom-precise level. This perspective has been promoted in recent literature by us and others.[21a,b,24]

Acknowledgements

This work was funded by the German Research Foundation (DFG) within a Reinhard Koselleck Project (FI 502/44-1). Support by the TUM Graduate School is acknowledged. H. L. thanks the China Scholarship Council for a Ph.D. grant. S. K. and J.-Y. S. are grateful to GENCI (Grand Equipment National de Calcul Intensif) for HPC resources (Project A0050807367). The authors thank Jürgen Kudermann for GC measurements. We are grateful to Brigitte Breitenstein (LMU) and Prof. Konstantin Karaghiosoff (LMU) for recording and support by interpretation of NMR spectra. Yannick Coppel (LCC CRNS Toulouse) is acknowledged for discussion on NOESY and ROESY data interpretation. Open Access funding enabled and organized by Projekt DEAL.

Conflict of Interest

The authors declare no conflict of interest.

Data Availability Statement

The data that support the findings of this study are available from the corresponding author upon reasonable request.

Keywords: (Poly-) Hydrides · Density Functional Calculations · Metal Cluster · ROESY · Semihydrogenation Catalysis

[1] a) J. Campos, *Nat. Chem. Rev.* **2020**, *4*, 696–702; b) K. Mayer, J. Weßing, T. F. Fässler, R. A. Fischer, *Angew. Chem. Int. Ed.* **2018**, *57*, 14372–14393; c) M. Schütz, C. Gemel, W. Klein, R. A. Fischer, T. F. Fässler, *Chem. Soc. Rev.* **2021**, *50*, 8496–8510.
[2] T. Cadenbach, C. Gemel, R. Schmid, R. A. Fischer, *J. Am. Chem. Soc.* **2005**, *127*, 17068–17078.

[3] T. Steinke, M. Cokoja, C. Gemel, A. Kempter, A. Krapp, G. Frenking, U. Zenneck, R. A. Fischer, *Angew. Chem. Int. Ed.* **2005**, *44*, 2943–2946.
[4] T. Steinke, C. Gemel, M. Cokoja, M. Winter, R. A. Fischer, *Angew. Chem. Int. Ed.* **2004**, *43*, 2299–2302.
[5] M. Muhr, R. Bühler, H. Liang, J. Gilch, C. Jandl, S. Kahlal, J.-Y. Saillard, C. Gemel, R. A. Fischer, *Chem. Eur. J.* **2022**, *28*, e202200887.
[6] In a different approach the catalytic activity of TM centres has been modified by positioning a Lewis-acidic E(III) centre in close proximity. This achieved by the use of sophistically tailored pincer-type ligands: a) R. Seki, N. Hara, T. Saito, Y. Nakao, *J. Am. Chem. Soc.* **2021**, *143*, 6388–6394; b) M. V. Vollmer, J. Ye, J. C. Linehan, B. J. Graziano, A. Preston, E. S. Wiedner, C. C. Lu, *ACS Catal.* **2020**, *10*, 2459–2470; c) I. Fujii, K. Semba, Q.-Z. Li, S. Sakaki, Y. Nakao, *J. Am. Chem. Soc.* **2020**, *142*, 11647–11652; d) R. Yamada, N. Iwasawa, J. Takaya, *Angew. Chem. Int. Ed.* **2019**, *58*, 17251–17254; e) H. Kameo, J. Yamamoto, A. Asada, H. Nakazawa, H. Matsuzaka, D. Bourissou, *Angew. Chem. Int. Ed.* **2019**, *58*, 18783–18787; f) J. Takaya, N. Iwasawa, *J. Am. Chem. Soc.* **2017**, *139*, 6074–6077; g) J. Takaya, *Chem. Sci.* **2021**, *12*, 1964–1981; h) W.-C. Shih, O. V. Ozerov, *J. Am. Chem. Soc.* **2017**, *139*, 17297–17300; i) J. Fajardo, J. C. Peters, *J. Am. Chem. Soc.* **2017**, *139*, 16105–16108; j) R. C. Cammarota, C. C. Lu, *J. Am. Chem. Soc.* **2015**, *137*, 12486–12489; k) R. C. Cammarota, M. V. Vollmer, J. Xie, J. Ye, J. C. Linehan, S. A. Burgess, A. M. Appel, L. Gagliardi, C. C. Lu, *J. Am. Chem. Soc.* **2017**, *139*, 14244–14250.
[7] a) P. Heiß, J. Hornung, C. Gemel, R. A. Fischer, *Chem. Commun.* **2022**, *58*, 4332–4335; b) M. Muhr, J. Hornung, J. Weßing, C. Jandl, C. Gemel, R. A. Fischer, *Inorg. Chem.* **2020**, *59*, 5086–5092; c) M. Molon, C. Gemel, P. Jerabek, L. Trombach, G. Frenking, R. A. Fischer, *Inorg. Chem.* **2014**, *53*, 10403–10411.
[8] J. F. Hartwig, in *Organotransition metal chemistry: from bonding to catalysis*, University Science Books, Sausalito, **2010**.
[9] a) H. Zea, K. Lester, A. K. Datye, E. Rightor, R. Gulotty, W. Waterman, M. Smith, *Appl. Catal. A* **2005**, *282*, 237–245; b) C. N. Thanh, B. Didillon, P. Sarrazin, C. Cameron, *U. S. Patent 6054409A* **2000**.
[10] a) M. A. Rahim, J. Tang, A. J. Christofferson, P. V. Kumar, N. Meftahi, F. Centurion, Z. Cao, J. Tang, M. Baharfar, M. Mayyas, F.-M. Allioux, P. Koshy, T. Daeneke, C. F. McConville, R. B. Kaner, S. P. Russo, K. Kalantar-Zadeh, *Nat. Chem.* **2022** *14*, 935–941; b) J. Prinz, C. A. Pignedoli, Q. S. Stöckl, M. Armbrüster, H. Brune, O. Gröning, R. Widmer, D. Passerone, *J. Am. Chem. Soc.* **2014**, *136*, 11792–11798; c) K. Kovnir, M. Armbrüster, D. Teschner, T. V. Venkov, F. C. Jentoft, A. Knop-Gericke, Y. Grin, R. Schlögl, *Sci. Technol. Adv. Mater.* **2007**, *8*, 420–427.
[11] a) Y. Cao, H. Zhang, S. Ji, Z. Sui, Z. Jiang, D. Wang, F. Zaera, X. Zhou, X. Duan, Y. Li, *Angew. Chem. Int. Ed.* **2020**, *59*, 11647–11652; b) K. Schütte, A. Doddi, C. Kroll, H. Meyer, C. Wiktor, C. Gemel, G. van Tendeloo, R. A. Fischer, C. Janiak, *Nanoscale* **2014**, *6*, 5532–5544; c) C. Li, Y. Chen, S. Zhang, J. Zhou, F. Wang, S. He, M. Wei, D. G. Evans, X. Duan, *ChemCatChem* **2014**, *6*, 824–831; d) F. Studt, F. Abild-Pedersen, T. Bligaard, R. Z. Sørensen, C. H. Christensen, J. K. Nørskov, *Science* **2008**, *320*, 1320–1322.
[12] A. Seifert, G. Linti, *Eur. J. Inorg. Chem.* **2007**, 5080–5086.
[13] a) A. Seifert, G. Linti, *Inorg. Chem.* **2008**, *47*, 11398–11404; b) M. Muhr, P. Heiß, M. Schütz, R. Bühler, C. Gemel, M. H. Linden, H. B. Linden, R. A. Fischer, *Dalton Trans.* **2021**, *50*, 9031–9036.
[14] J. H. J. Berthel, M. W. Kuntze-Fechner, U. Radius, *Eur. J. Inorg. Chem.* **2019**, 2618–2623.
[15] J. C. Calabrese, L. F. Dahl, A. Cavalieri, P. Chini, G. Longoni, S. Martinengo, *J. Am. Chem. Soc.* **1974**, *96*, 2616–2618.
[16] a) J. Hornung, J. Weßing, P. Jerabek, C. Gemel, A. Pöthig, G. Frenking, R. A. Fischer, *Inorg. Chem.* **2018**, *57*, 12657–12664; b) T. Cadenbach, C. Gemel, R. Schmid, M. Halbherr, K. Yusenko, M. Cokoja, R. A. Fischer, *Angew. Chem. Int. Ed.* **2009**, *48*, 3872–3876; c) T. Steinke, C. Gemel, M. Winter, R. A. Fischer, *Chem. Eur. J.* **2005**, *11*, 1636–1646; d) P. Jutzi, B. Neumann, L. O. Schebaum, A. Stammler, H.-G. Stammler, *Organometallics* **1999**, *18*, 4462–4464.
[17] J. Y. C. Chen, A. A. Martí, N. J. Turro, K. Komatsu, Y. Murata, R. G. Lawler, *J. Phys. Chem. B* **2010**, *114*, 14689–14695.
[18] a) D. G. Hamilton, R. H. Crabtree, *J. Am. Chem. Soc.* **1988**, *110*, 4126–4133; b) J. Campos, L. S. Sharninghausen, R. H. Crabtree, D. Balcells, *Angew. Chem. Int. Ed.* **2014**, *53*, 12808–12811.
[19] T. Pery, K. Pelzer, G. Buntkowsky, K. Philippot, H.-H. Limbach, B. Chaudret, *ChemPhysChem* **2005**, *6*, 605–607.
[20] M. Krajčí, J. Hafner, *ChemCatChem* **2016**, *8*, 34–48.
[21] a) O. P. E. Townrow, C. Chung, S. A. Macgregor, A. S. Weller, J. M. Goicoechea, *J. Am. Chem. Soc.* **2020**, *142*, 18330–18335; b) O. P. E. Townrow, S. B. Duckett, A. S. Weller, J. M. Goicoechea, *Chem. Sci.* **2022**, *13*, 7626–7633; c) J. A. Widegren, R. G. Finke, *J. Mol. Catal. A* **2003**, *198*, 317–341.
[22] M. Krajčí, J. Hafner, *J. Phys. Chem. C* **2014**, *118*, 12285–12301.
[23] a) M.-M. Zhang, X.-Y. Dong, Z.-Y. Wang, H.-Y. Li, S.-J. Li, X. Zhao, S.-Q. Zang, *Angew. Chem. Int. Ed.* **2020**, *59*, 10052–10058; b) X.-K. Wan, X.-L. Cheng, Q. Tang, Y.-Z. Han, G. Hu, D.-e. Jiang, Q.-M. Wang, *J. Am. Chem. Soc.* **2017**, *139*, 9451–9454; c) S.-D. Bian, H.-B. Wu, Q.-M. Wang, *Angew. Chem. Int. Ed.* **2009**, *48*, 5363–5365.
[24] a) J. Hornung, M. Muhr, C. Gemel, R. A. Fischer, *Dalton Trans.* **2019**, *48*, 11743–11748; b) C. Ganesamoorthy, J. Wessing, C. Kroll, R. W. Seidel, C. Gemel, R. A. Fischer, *Angew. Chem. Int. Ed.* **2014**, *53*, 7943–7947; c) M. Schütz, C. Gemel, M. Muhr, C. Jandl, S. Kahlal, J.-Y. Saillard, R. A. Fischer, *Chem. Sci.* **2021**, *12*, 6588–6599; d) J. Weßing, C. Ganesamoorthy, S. Kahlal, R. Marchal, C. Gemel, O. Cador, A. C. H. Da Silva, J. L. F. Da Silva, J.-Y. Saillard, R. A. Fischer, *Angew. Chem. Int. Ed.* **2018**, *57*, 14630–14634.
[25] Deposition number 2180123 contains the supplementary crystallographic data for this paper. These data are provided free of charge by the joint Cambridge Crystallographic Data Centre and Fachinformationszentrum Karlsruhe Access Structures service.

Manuscript received: June 22, 2023
Accepted manuscript online: July 5, 2023
Version of record online: July 28, 2023